Journal of
Nanoscience and Nanotechnology
Vol. 10, 2017–2022, 2010

Preparation and Far Infrared Emission Properties of Natural Sepiolite Nanofibers

Fei Wang, Jinsheng Liang*, Qingguo Tang, Liwei Li, and Lijun Han

Institute of Power Source and Ecomaterials Science, Hebei University of Technology, Box 1055, Tianjin 300130, China

Sepiolite nanofibers were prepared by high-speed air current superfine technique, using natural sepiolite samples as raw materials. Through characterization by scanning electron microscope (SEM), X-ray diffraction (XRD), dynamic contact angle meter and tensiometer (DCAMT) and Fourier transform infrared spectroscope (FTIR), it was found that the defibered sepiolite nanofibers with an average diameter of about 100 nm and length greater than 9 μm had a better far infrared emitting performance than acid-purified sepiolite as the contrast sample, and the defibering treatment led to the improvement of far infrared emitting performance of sepiolite due to the increase of surface free energy, the increase of infrared active bond vibrations, and the decrease of cell volume caused by the distortion of structural channel.

Keywords: Sepiolite, Far Infrared Emission, Nanofibers, Mineral Materials, Defiber.

1. INTRODUCTION

Ever since the discovery of carbon nanotubes by Iijima, there has been great interest in the synthesis and characterization of other one-dimensional structures.[1] Due to their characteristic one-dimensional nanostructures, nanofibers have recently attracted widespread interest for their potential applications in many fields.[2–4] These nanofibers have been prepared by various synthetic procedures such as template synthesis and electrospinning.[5–8] However, these methods often involve a series of complicated procedures and the use of expensive and sensitive agents. An alternative to obtaining nanofibers is to process minerals, which may be simple and cheap.

Sepiolite is a sort of fibrous silicate clay mineral rich in magnesium with a unit cell formula of $Si_{12}O_{30}Mg_8(OH)_4(H_2O)_4 \cdot 8H_2O$, which has fine microporous channels with dimensions of 0.37×1.06 nm running parallel to the length of the fibers and high interior surface area of 300 m^2/g.[9–12] Due to the characteristics of large reservation, low cost, high efficiency, and reusability, sepiolite has been studied by many scientists in the field of environmental pollution control in recent years.[13–15] Sepiolite usually occurs as large bundles of crystalline fibers about 10–5000 nm long, 10–30 nm wide, and 5–10 nm thick, and effective defibering treatment for sepiolite could obtain the natural nanofibers.[15–17] However, to the best of our knowledge, the preparation of sepiolite nanofibers has not been reported.

The infrared technique has been widely used in the fields of military, aviation, astronavigation, communications, medical treatment, and agriculture. In recent years, the far infrared functional materials have been also well used in environment protection and energy saving.[18] Far infrared materials obtained by sintering many kinds of metal oxides are usually costly. Natural minerals are the basic materials for the preparation of far infrared functional materials, which have excellent physiochemical properties and prominent value advantage. The far infrared emitting performance of granular materials has been widely studied,[19,20] however, there are few reports about the far infrared emitting performance of fibrous materials.

In this paper, the sepiolite nanofibers were prepared by means of the high-speed air current superfine technique, using natural sepiolite samples as raw materials. The relationships between the far infrared emitting performance and microstructure, crystal structure, and surface free energy were fully investigated using acid purified sepiolite as the contrast sample, which established a theoretical and experimental basis for the far infrared emitting performance of sepiolite nanofibers.

*Author to whom correspondence should be addressed.

2. EXPERIMENTAL DETAILS

2.1. Sample Preparation

Experimental details were as follows. First, 500.00 g of natural sepiolite samples (chemical composition in mass ratio are as follows: SiO_2, 54.36%; MgO, 35.56%; CaO, 5.67%; Fe_2O_3, 1.36%; Total amount 96.95%) were added into 3500 ml of water solution containing 175 ml of hydrochloric acid. Second, the mixture was stirred at the speed of 2,000 rpm for 2 h by a high-speed dispersing machine, and then the sepiolite solid was separated from the admixture by vacuum filtering and washed several times with distilled water until Cl^- was not tested with $AgNO_3$, dried at 60 °C, and then the dry cake was crushed and ground into powders using 20 mesh sieves. Then, the above acid-purified sepiolite samples were superfined by jet mill grinding. The grinding room air pressure is controlled between 0.7 and 0.85 MPa, the bearing protection air pressure is 0.2 MPa, the wash air pressure is 0.15 MPa, and the feeding rate is from 2 to 12 kg/h.

2.2. Sample Characterization

The microstructure of the samples was observed by scanning electron microscopy (Philips-XL30) at 25.0 kV and 30 μA, and the X-ray diffraction (XRD) analysis was performed on a Philips-DMAX-2500 with Cu Kα radiation. The surface tension of the samples was obtained by a dynamic contact angle meter and tensiometer (Germany Dataphysics DCAT21), which can be used to calculate the surface free energy according to Ref. [21].

The Fourier transform infrared spectrum (FTIR) was obtained using a BRUKER-80V made in Germany using KBr discs. The far infrared emissivity of the samples was also evaluated by a BRUKER-80V made in Germany.

2.3. Bulk Density of Samples

The bulk density of samples was determined by measuring the mass of a fixed volume. A fixed volume, i.e., a glass cylinder, was filled with the samples without vibration in accordance to the China Standard Test Methods (GB/T 16913.3-1997).

3. RESULTS AND DISCUSSION

3.1. Effect of Feeding Rate on Bulk Density of Sepiolite

Figure 1 shows the variation of bulk density of sepiolite after grinding at different feeding rates from 2 to 12 kg/h.

Figure 1 shows that the sepiolite after grinding at the feeding rate of 6 kg/h has the lowest bulk density of 0.0352 g/cm^3. For powders with very small particle size, the smaller the particle size, the lower their bulk density.[22]

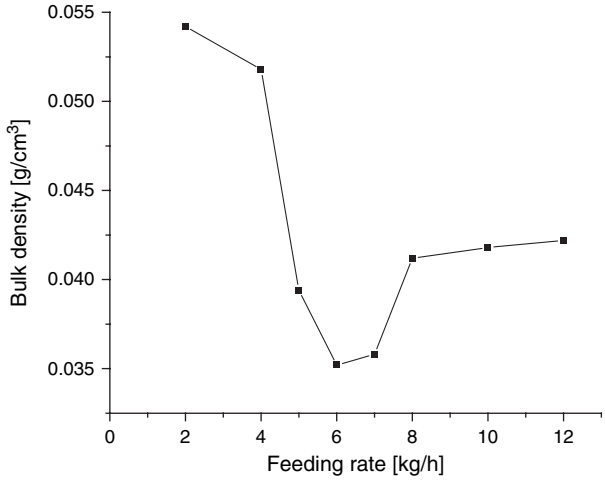

Fig. 1. Variation of bulk density of sepiolite after grinding at different feeding rates.

Therefore, the sepiolite samples after grinding at the feeding rate of 6 kg/h have the smallest geometric mean particle diameter, which can be explained as follows. The jet mill is a static machine, which does not have any grinding media. The milling component of the jet mill consists of a chamber with nozzles. The sepiolite samples to be pulverized are accelerated by pressurized gas jets, and the grinding effect is produced by interparticle collision or impact between the particles and the inner wall, as

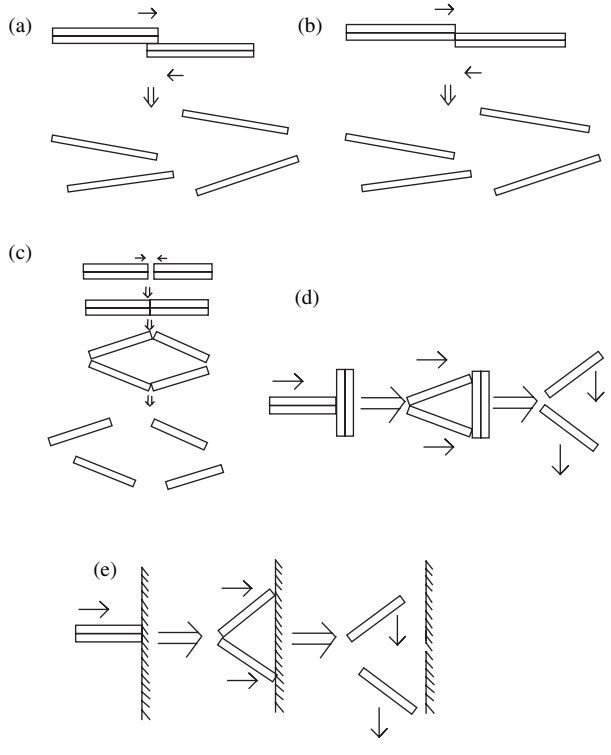

Fig. 2. Schematic pictures of collision forms in the process of defibering for sepiolite: (a–d) interparticle collision forms, and (e) collision form between particle and inner wall.

shown in Figure 2. The low feeding rate is beneficial for impact between the particles and the inner wall, which can be seen in Figure 2(e), but the interparticle collision, as shown in Figure 2(a–d), is useless at very low feeding rate. When the feeding rate is 6 kg/h, impact between particle and inner wall and interparticle collision are perfect for the defibering treatment. According to the above analysis, 6 kg/h is selected as the grinding feeding rate for the acid purified sepiolite in order to obtain the smallest geometric mean particle diameter of sepiolite samples.

3.2. Microstructure of Sepiolite Nanofibers

Figure 3 shows the microstructure of acid-purified sepiolite and defibered sepiolite nanofibers.

From Figure 3(b), it can be seen that the sepiolite keeps its fibrous micro-morphology after defibering treatment due to its specific crystal structure and grinding by jet mill, which does not have any grinding media. However, the defibered sepiolite nanofibers with an average diameter of about 100 nm and length greater than 9 μm keep a stable length and become obviously thinner than acid-purified sepiolite (Fig. 3(a)) as the contrast sample, corresponding to what is shown in Figure 2.

3.3. Surface Free Energy of Sepiolite Nanofibers

Figure 4 shows the surface free energy of acid-purified sepiolite and defibered sepiolite nanofibers.

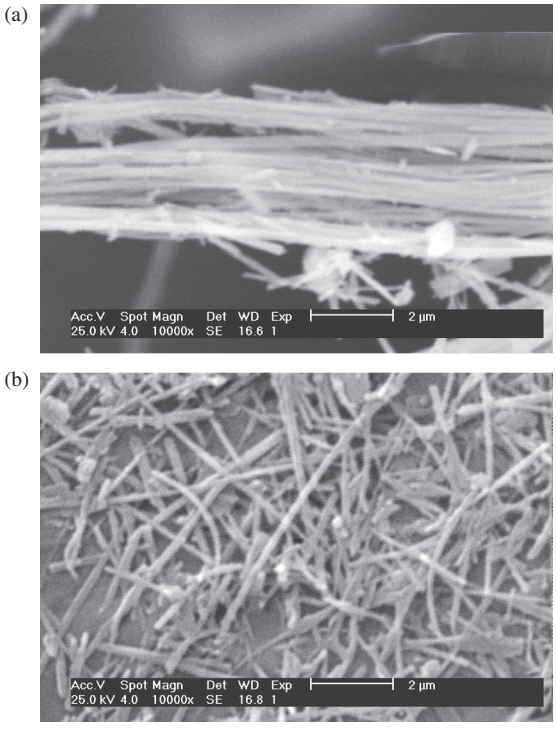

Fig. 3. Microstructure of sepiolite samples: (a) acid-purified sepiolite and (b) defibered sepiolite nanofibers.

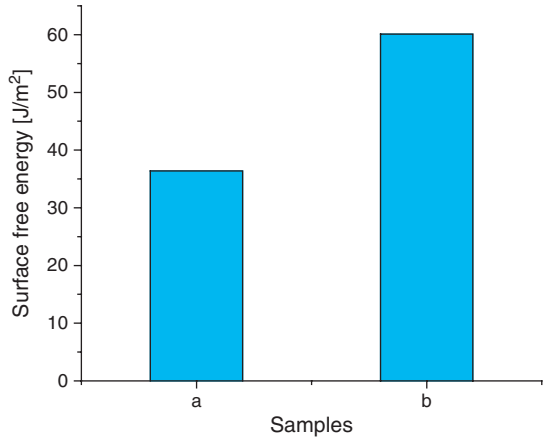

Fig. 4. Surface free energy of sepiolite samples: (a) acid-purified sepiolite and (b) defibered sepiolite nanofibers.

From Figure 4 we can see that the surface free energy of defibered sepiolite nanofibers is obviously higher than that of acid-purified sepiolite as the contrast sample, which may be due to the obvious decrease of geometric mean particle diameter and distortion of structural channel caused by shearing force during the defibering treatment of sepiolite.

3.4. Cell Volume of Sepiolite Nanofibers

Figure 5 shows the XRD patterns of acid-purified sepiolite and defibered sepiolite nanofibers.

From Figure 5, it can be seen that some peaks in every sample are in agreement with literature data for pure sepiolite [d-spacings and $\{hkl\}$ values: 1.210 (110), 0.747 (130), 0.673 (040), etc; space group: Pncn (52); JCPDS No. 13-0595]. From Figure 5(b) we can see that the characteristic diffraction peaks broaden subtly after defibering treatment, which may be due to the distortion of lattice and decrease of the aggregation of fibers.[23] From Figure 5 we can also see that the main crystal structure of all sepiolite samples does not change apparently and no new phase is formed. Some peaks of sepiolite move toward higher degrees after defibering treatment, indicating that the unit cell of sepiolite begins to shrink. In detail, Table I lists the lattice parameters (a, b, and c axes) of sepiolite analyzed by Jade 5.0 software, and unit cell volumes (V_{cell}) of sepiolite calculated through Formula (1), whose original data come from the XRD patterns in Figure 5.

$$V_{cell} = a \times b \times c \quad (1)$$

From Table I, we can see that the unit cell volume (V_{cell}) of defibered sepiolite nanofibers decreases by 0.6% compared with that of acid-purified sepiolite, mainly due to the decrease of lattice parameters (a and b axes) of defibered sepiolite nanofibers, and we can also see the distortion of the structural channel due to the rotation of the basic structural unit in the defibering process, which is shown in Figure 6.

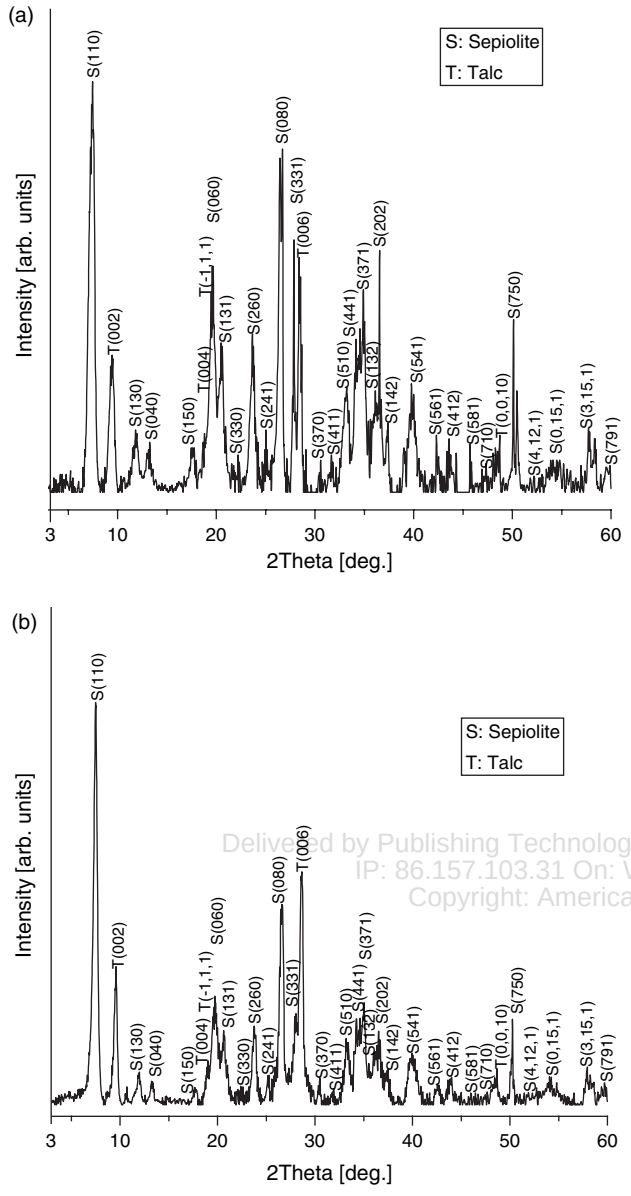

Fig. 5. XRD patterns of sepiolite samples: (a) acid-purified sepiolite and (b) defibered sepiolite nanofibers.

3.5. Far Infrared Absorption Spectra of Sepiolite Nanofibers

Figure 7 shows the FTIR spectra of acid-purified sepiolite and defibered sepiolite nanofibers.

From Figure 7, it can be seen that FTIR spectrum of acid-purified sepiolite has many absorption peaks. The

Table I. Lattice parameters from XRD patterns for sepiolite: (a) acid purified sepiolite and (b) defibered sepiolite nanofibers.

Sample	a (nm)	b (nm)	c (nm)	V_{cell} (nm^3)
a	1.353	2.705	0.525	1.921
b	1.349	2.692	0.526	1.909

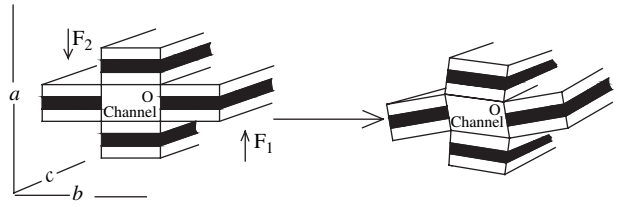

Fig. 6. Schematic picture of the distortion of the structural channel in the process of defibering sepiolite (F_1 and F_2: shearing force).

Mg_3OH band at 3680 cm^{-1} characterized by low bonding strength is ascribed to the presence of hydroxyl in the octahedral sheet and the hydroxyl stretching vibration in the external surface of sepiolite. On the other hand, the 3565 and 3400 cm^{-1} bands are respectively assigned to the hydroxyl stretching, representing the zeolitic water in the channels, and bound water coordinated to magnesium in the octahedral sheet. The bands at 1661 and 664 cm^{-1} developed due to the hydroxyl bending vibrations again reflect the presence of bound water. These above-mentioned bands are not significantly changed after defibering treatment. However, the Si–O combination bands at 1210, 1074, and 977 cm^{-1} formed as a result of the Si–O vibrations and the deep bands at 1020 and 470 cm^{-1} ascribed to the stretching of Si–O in the Si–O–Si groups of the tetrahedral sheet become sharper and deeper after defibering treatment, indicating the increase of infrared active bond vibrations and far infrared emitting performance.[24–26]

3.6. Far Infrared Emissivity of Sepiolite Nanofibers

According to Kirchhoff's Radiation Law, the material absorptivity (α) is equal to its emissivity (ε) under conditions of same temperature and incident wave. That is, the higher the material absorption peak, the higher its far

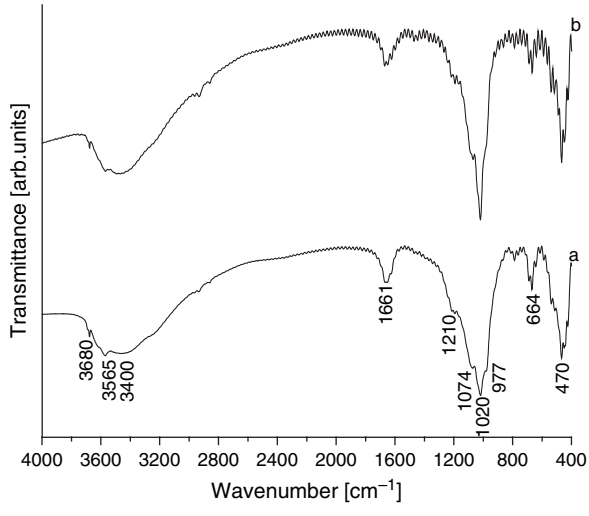

Fig. 7. FTIR spectra of sepiolite samples: (a) acid-purified sepiolite and (b) defibered sepiolite nanofibers.

infrared emissivity. However, the far infrared absorption spectrum of the material is not quite coincident with that of far infrared emissivity due to the influence of its shape, granularity, and density. The far infrared emitting performance of material is often evaluated by its emissivity in practice. Figure 8 shows the far infrared emissivity patterns and radiant energy patterns of samples.

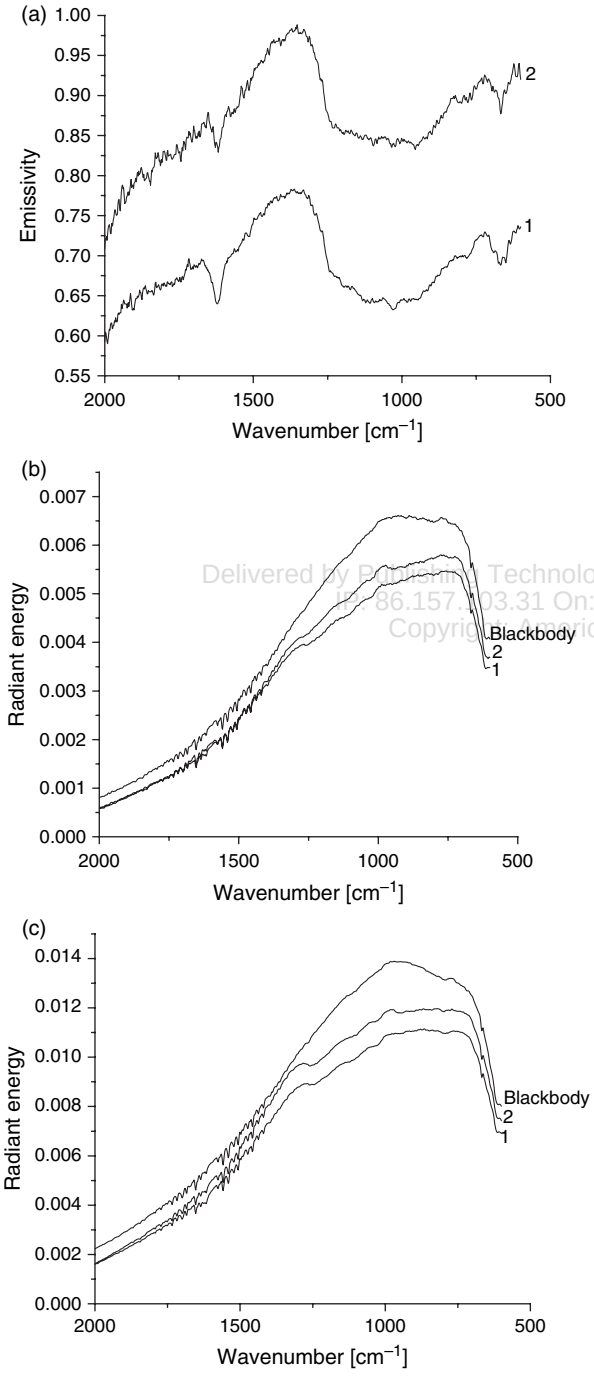

Fig. 8. Far infrared emissivity patterns and radiant energy patterns of samples. (a) emissivity patterns, (b) radiant energy patterns at 80 °C, (c) radiant energy patterns at 120 °C, (1) acid-purified sepiolite, and (2) defibered sepiolite nanofibers.

From Figure 8(a), it can be seen that the far infrared emissivity of defibered sepiolite nanofibers between 2000 and 600 cm^{-1} is improved compared with acid-purified sepiolite, in agreement with the results of surface free energy (Fig. 4), which shows that the increase of surface free energy is propitious to the improvement of far infrared emitting performance of material. From Figures 8(b and c), it can be seen that radiant energy of defibered sepiolite nanofibers at different temperatures between 1210 and 600 cm^{-1} is obviously enhanced compared with acid-purified sepiolite, in agreement with the results of FTIR spectra (Fig. 7), showing that the increase of infrared active bond vibrations is propitious to the improvement of far infrared emitting performance and radiant energy of material. The main reasons that defibering treatment can improve the far infrared emitting performance of sepiolite samples can be summarized as follows. First, in general, the increase of surface free energy is advantageous for the transition of particles, including atoms, electrons, and molecules, from low-energy level to high-energy level. However, they fall down to low-energy level again just a short time later, and at the same time, the surplus energy is mainly given off in the form of electromagnetic radiation—far infrared radiation is also given off—thus resulting in the improvement of far infrared emitting performance of material.

Second, according to Kirchhoff's Law, at the same temperature, every substance has the same ratio of the monochromatic radiant exitance and monochromatic adsorption with corresponding wave. Therefore, the increase of infrared active bond vibrations is propitious to the improvement of radiant energy and far infrared emitting performance of the material.

Third, generally, the crystal structure is closely related to far infrared emitting performance of the material in that the crystal structure is bound together depending on the elastic force in terms of classic physical theory. From lattice dynamics, it can be seen that the effect of the crystal structure on far infrared emitting performance of the material is evaluated through atomic three-dimensional lattice vibrations.[27] The decrease of cell volume leading to the variation of the lattice spectrum is propitious to the improvement of the far infrared emitting performance of sepiolite samples.

4. CONCLUSIONS

In this paper, we have described a novel and simple approach to prepare sepiolite nanofibers with an average diameter of about 100 nm and length greater than 9 μm grinding at the feeding rate of 6 kg/h by the high-speed air current superfine technique. The defibering treatment of sepiolite is propitious to the increase of surface free energy, the increase of infrared active bond vibrations, and the decrease of cell volume caused by the distortion of

structural channel, thus leading to the improvement of its far infrared emitting performance.

Acknowledgments: This research was financially supported by the National Science and Technology Support Planning Project of the Republic of China (Grant No. 2008BAE60B07).

References and Notes

1. S. Iijima, *Nature* 354, 56 **(1991)**.
2. D. J. Yang, Z. F. Zheng, H. Y. Zhu, H. W. Liu, and X. P. Gao, *Adv. Mater*. 20, 2777 **(2008)**.
3. S. Virji, J. X. Huang, R. B. Kaner, and B. H. Weiller, *Nano Lett*. 4, 491 **(2004)**.
4. W. P. Hu, H. Nakashima, K. Furukawa, Y. Kashimura, K. Ajito, and K. Torimitsu, *Appl. Phys. Lett*. 85, 115 **(2004)**.
5. H. L. Wang and L. M. Qi, *Adv. Mater*. 18, 1249 **(2008)**.
6. M. B. Zheng, J. M. Cao, X. F. Ke, G. B. Ji, Y. P. Chen, K. Shen, and J. Tao, *Carbon* 45, 1111 **(2007)**.
7. M. Graeser, M. Bognitzki, W. Massa, C. Pietzonka, A. Greiner, and J. H. Wendorff, *Adv. Mater*. 19, 4244 **(2007)**.
8. D. Li and Y. N. Xia, *Nano Lett.* 3, 555 **(2003)**.
9. G. Rytwo, D. Tropp, and C. Serban, *Appl. Clay Sci*. 20, 273 **(2002)**.
10. G. Sandi, R. E. Winans, S. Seifert, and K. A. Carrado, *Chem. Mater*. 14, 739 **(2002)**.
11. A. Esteban-Cubillo, R. Pina-Zapardiel, J. S. Moya, M. F. Barba, and C. Pecharroman, *J. Eur. Ceram. Soc*. 28, 1763 **(2008)**.
12. A. Sun, J. B. Caillerie, and J. J. Fripiat, *Microporous Mater*. 5, 135 **(1995)**.
13. M. F. Brigatti, C. Lugli, and L. Poppi, *Appl. Clay Sci*. 16, 45 **(2000)**.
14. S. Mendioroz, M. I. Guijarro, P. J. Bermejo, and V. Munoz, *Environ. Sci. Technol*. 33, 1697 **(1999)**.
15. M. Molina-Sabio, J. C. Gonzalez, and F. Rodriguez-Reinoso, *Carbon* 42, 448 **(2004)**.
16. F. Rodriguez-Reinoso, M. Molina-Sabio, and J. C. Gonzalez, *Carbon* 39, 776 **(2001)**.
17. R. H. Eduardo, *J. Mater. Chem*. 11, 86 **(2001)**.
18. J. S. Liang, D. B. Zhu, J. P. Meng, L. J. Wang, F. P. Li, Z. G. Liu, Y. Ding, L. H. Liu, and G. C. Liang, *J. Nanosci. Nanotechnol*. 8, 1203 **(2008)**.
19. J. M. Tsay, M. Pflughoefft, L. A. Bentolila, and S. Weiss, *J. Am. Chem. Soc*. 126, 1926 **(2004)**.
20. J. P. Meng, J. S. Liang, X. Q. Ou, Y. Ding, and G. C. Liang, *J. Nanosci. Nanotechnol*. 8, 1279 **(2008)**.
21. L. Cerne, B. Simoncic, and M. Zeljko, *Appl. Surf. Sci*. 254, 6467 **(2008)**.
22. S. Mani, L. G. Tabil, and S. Sokhansanj, *Biomass Bioenergy* 27, 339 **(2004)**.
23. H. X. Chen, M. S. Zheng, H. Y. Sun, and Q. M. Jia, *Mater. Sci. Eng., A* 445–446, 725 **(2007)**.
24. A. V. Miguel, S. Mercedes, A. B. Miguel, and D. L. Juan, *Spectrochim. Acta., A* 52, 1685 **(1996)**.
25. E. Sabah and M. S. Celik, *J. Colloid Interface Sci*. 251, 33 **(2002)**.
26. R. L. Frost, O. B. Locos, H. Ruan, and J. T. Kloprogge, *Vib. Spectrosc*. 27, 1 **(2001)**.
27. K. Huang, Solid State Physics, Higher Education Press in China, Beijing **(2001)**.

Received: 8 November 2008. Accepted: 7 April 2009.